Pairing and phase separation in a one-dimensional spin-bag liquid

Piotr Wróbel*
Department of Physics, Loomis Laboratory of Physics, University of Illinois at Urbana-Champaign, 1110 West Green Street, Urbana, Illinois 61801

Robert Eder
Department of Applied and Solid State Physics, University of Groningen, The Netherlands
(Received 11 December 1995; revised manuscript received 22 July 1996)

We study the one-dimensional t-J model in a staggered magnetic field by a variational calculation based on the string picture. Our key assumption is the separation of energy scales between rapid incoherent hole motion on scale t and slow coherent motion on scale J. We discuss pair formation and phase separation in the hole liquid and find good agreement with exact diagonalization of small clusters. [S0163-1829(96)01045-4]

I. INTRODUCTION

The discovery of high-temperature superconductivity (HTSC) in layered copper oxides has stimulated considerable attention in systems of strongly interacting fermions during the last years. A challenging question is whether simple planar models, such as the two-dimensional (2D) t-J Hamiltonian, can give some insight into the nature of carriers responsible for HTSC. It is well established that two holes in a finite 2D cluster t-J model form a bound state if J is larger than a critical value.[1–3] This immediately suggests the question of whether this implies either hole pairing or phase separation in an infinite system (or whether the binding is a finite-size effect altogether). In the 2D clusters which are amenable to exact diagonalization, the surface of the cluster is an appreciable fraction of the total volume. Therefore it seems natural to seek and study a 1D analog of the 2D t-J model. Alas, the 1D t-J model belongs to the universality class of Luttinger liquids[4–6] and hence may exhibit quite different behavior than its 2D counterpart. On the other hand, by extending the 1D t-J model by a term which corresponds to the interaction of electron spins with a staggered magnetic field which stabilizes the long-range antiferromagnetic order likely present in higher dimensions at low doping, one may hope to get an analog of the 2D t-J model. We therefore study the Hamiltonian $H=H_t+H_{\mathrm{Ising}}+H_1$ with

$$H_t=-t\sum_{\langle i,j\rangle,\sigma}(\hat{c}^{\dagger}_{i,\sigma}\hat{c}_{j,\sigma}+\mathrm{H.c.}),$$

$$H_{\mathrm{Ising}}=J\sum_{\langle i,j\rangle}\left(S^z_iS^z_j-\frac{\hat{n}_i\hat{n}_j}{4}\right)-h\sum_l(-1)^lS^z_l,$$

$$H_1=\frac{J}{2}\sum_{\langle i,j\rangle}(S^+_iS^-_j+\mathrm{H.c.}). \tag{1}$$

The operators $\hat{c}^{\dagger}_{i,\sigma}$ are expressed in terms of ordinary fermion operators as $c^{\dagger}_{i,\sigma}(1-n_{i,-\sigma})$. That model was introduced and discussed by Bonča *et al.*[7] who investigated it by means of exact diagonalization, a continuum approximation in the $J,h\ll t$ limit, and a high-field expansion in the $h\gg t$ limit. Numerical results by those authors suggest that even a modest staggered field induces the formation of bound pairs in a range of parameters.

Our aim is to study the quasiparticles and their interaction in the moderately doped model (1) by comparing the results of exact diagonalization with an analysis in the framework of the string or spin bag approach. The method used in the variational part of our calculation seems to be a reliable analytical approach for the investigation of the moderately doped 2D t-J model in the physical regime of t/J. In addition to the predictions for the binding energy of two holes[8,9] which have subsequently been confirmed by numerical calculations,[10] there is recently an increasing number of numerical works[11] which verify another key prediction[12] of this approach, namely, the hole pocketlike Fermi surface.

The basic assumption of our variational calculation is a pronounced separation of energy scales in the motion of the doped holes. It is well known that in dimensions $D\geqslant 2$ a mobile hole which is created at some site i in a Néel-ordered spin state feels an ''effective potential'' due to the formation of ''strings.''[13,14] This is very different from 1D, where a hole created in a 1D Néel state may be thought of as decaying into a ''magnetic domain wall'' and a ''charged domain wall'' which may separate and propagate independently of each other; this is in fact the most simple visualization of spin charge separation. The staggered magnetic field then creates a linearly ascending potential between the two domain walls also in 1D, and thus provides the attractive interaction between ''holon'' and ''spinon'' which may be inherent to higher dimensions. It is only due to the relaxation of the defect string by means of the quantum fluctuations of the spin system that coherent hole propagation becomes possible. The key feature of hole motion therefore is the superposition of two very different dynamics: the rapid incoherent zigzag motion of the self-trapped hole on an energy scale $\sim t$ and, superimposed onto this, the coherent motion on an energy scale $\sim J$ which is enabled by the relaxation of the ''strings.'' An obvious manifestation of this separation of energy scales is the fact[2] that the creation of a single hole in an antiferromagnet lowers the kinetic energy by the large and nearly $\boldsymbol{k}$-independent amount $\sim 3t$ (which stems from the

incoherent zigzag motion) whereas the dispersion of the low-energy states (which stems from the coherent motion) rigorously scales with J.

II. VARIATIONAL TREATMENT OF HOLE MOTION

In order to describe the twofold dynamics of the holes, i.e., the superposition of rapid incoherent motion on scale t and slow coherent motion on scale J, we introduce the following definitions (A denotes the $\uparrow$ sublattice, B the $\downarrow$ sublattice):

$$T_{\pm}=\sum_{i\in A} c^{\dagger}_{i,\downarrow}c_{i\pm 1,\downarrow}+\sum_{i\in B} c^{\dagger}_{i,\uparrow}c_{i\pm 1,\uparrow}. \tag{2}$$

$T_{\pm}$ moves the hole by one lattice site in the positive or negative direction, and by construction decreases the staggered magnetization by 1. We next define the superoperator $L_{\pm}O=[T_{\pm},O]$ (where O denotes any operator) and the projection operator for $i\in A$, $P_i=\hat{n}_{i,\uparrow}\Pi_{j=i\pm 1}\hat{n}_{j,\downarrow}$ and for $j\in B$, $P_j=\hat{n}_{j,\downarrow}\Pi_{i=j\pm 1}\hat{n}_{i,\uparrow}$. Then, for $\nu\geqslant 0$ we define $A_{i,\pm\nu}=L^{\nu}_{\pm}c_{i,\uparrow}P_i$ (and an analogous definition for $j\in B$). The $A_{i,\pm\nu}$ create ''string states'' and obey $[M_S,A_{i,\pm\nu}]=-\nu A_{i,\pm\nu}$ where M_S is the operator of staggered magnetization. String states with the same ''initial site'' i are coupled by the hopping term; a superposition of such states therefore describes a hole trapped at the site i. As mentioned above the key assumption of our approach is the separation of energy scales between the rapid incoherent zigzag motion of the self-trapped holes and slow coherent motion mediated by the spin fluctuations. Thus, in a first step, we describe approximately the incoherent zigzag motion: We define a state with N_h holes trapped at the sites $i, j, \ldots, n$ by the ansatz

$$|\Psi_{i,j,\ldots,n}\rangle=\sum_{\mu,\nu,\ldots,\rho}\alpha^{i,j,\ldots,n}_{\mu,\nu,\ldots,\rho}A_{i,\nu}A_{j,\mu}\cdots A_{n,\rho}|AF\rangle. \tag{3}$$

The coefficients $\alpha^{i,j,\ldots,n}_{\mu,\nu,\ldots,\rho}$ are determined (approximately) such that $|\Psi_{i,j,\ldots,n}\rangle$ is an eigenstate of a Hamiltonian H' which represents dynamics of the self-trapped hole:

$$H'|\Psi_{i,j,\ldots,n}\rangle=E_{i,j,\ldots,n}|\Psi_{i,j,\ldots,n}\rangle. \tag{4}$$

In H' all processes which lead to relaxation of strings have been neglected. Since each hole is trapped within a typical length l around its starting point i, the holes will feel the presence of each other only if the distance of their starting points is smaller than l. In other words, if the distances between the ''starting points'' $i, j, \ldots, n$ in Eq. (3) are pairwise larger than l, Eq. (4) is solved to a good approximation by

$$\alpha^{i,j,\ldots,n}_{\mu,\nu,\ldots,\rho}=\tilde{\alpha}^{\tau_i}_{\mu}\tilde{\alpha}^{\tau_j}_{\nu}\cdots\tilde{\alpha}^{\tau_n}_{\rho}, \tag{5}$$

$$E_{i,j,\ldots,n}=\sum_i E^{\tau_i}_1, \tag{6}$$

where $\tilde{\alpha}^{\tau}_{\mu}$ (E^{τ}_1) are the expansion coefficients (eigenenergies) for the τth eigenstate of a *single* self-trapped hole, which can be computed from a 1D Schrödinger equation (see the Appendix).

Let us next assume that one pair of sites i, j is close to each other, but still far from all the other ones. In this case the two holes will feel the presence of each other, so that a different kind of Schrödinger equation for two holes has to be solved (see the Appendix). Then, the product of the two respective single-hole wave functions in Eq. (5) has to be replaced by the two-particle wave function, and analogously the sum of the two respective single-hole eigenvalues in Eq. (6) by the eigenvalue of the two-particle Schrödinger equation. This procedure is readily generalized to the case that more than two holes are ''clustering together'' or that there is more than one group of clustering holes. In this way, we obtain a systematic expansion in terms of two-particle, three-particle, . . . ,n-particle interactions between the dressed holes.

In the second step, we adiabatically couple configurations with different positions of the self-trapped holes. This means we now make the ansatz

$$|\Psi\rangle=\sum_{i,j,\ldots,n;\rho}\beta^{\rho}_{i,j,\ldots,n}|\Psi^{\rho}_{i,j,\ldots,n}\rangle, \tag{7}$$

which leads to the Schrödinger equation

$$H^{\rho_1,\rho_2}_{\vec{I}_1,\vec{I}_2}\beta^{\rho_2}_{\vec{I}_2}=EN^{\rho_1,\rho_2}_{\vec{I}_1,\vec{I}_2}\beta^{\rho_2}_{\vec{I}_2}. \tag{8}$$

Thereby we have introduced the overlap and Hamilton matrices

$$N^{\rho_1,\rho_2}_{(i_1,j_1,\ldots,n_1)(i_2,j_2,\ldots,n_2)}=\langle\Psi^{\rho_1}_{i_1,j_1,\ldots,n_1}|\Psi^{\rho_2}_{i_2,j_2,\ldots,n_2}\rangle, \tag{9}$$

$$H^{\rho_1,\rho_2}_{(i_1,j_1,\ldots,n_1)(i_2,j_2,\ldots,n_2)}=\langle\Psi^{\rho_1}_{i_1,j_1,\ldots,n_1}|H|\Psi^{\rho_2}_{i_2,j_2,\ldots,n_2}\rangle, \tag{10}$$

and introduced additional indices $\rho_{\ldots}$ which denote eigenstate indices of Eq. (4).

In the following, we will perform this procedure for single-hole states (which provide information about the energy associated with single-hole motion), two-hole states (which give information about the interaction between two holes, which may lead to pairing) and three-hole states (which is the minimum number of holes necessary to distinguish phase separation from hole pairing).

For a single-hole state with total momentum k, we must have $\beta^{\tau_i}_i\sim e^{ikR_i}$, so that the second step of the solution becomes trivial. The calculation of the $\tilde{\alpha}^{\tau}_{\nu}$ is shown in the Appendix.

The most difficult step then is the calculation of Eqs. (9) and (10). All processes which contribute to them have been represented by a kind of diagram depicted in Figs. 2–7. The open and solid circles in the right part of each figure represent the ''starting sites'' of holes for both wave functions which contribute to the matrix element and correspond to indices $i,j,\ldots,n$ in Eq. (3). The left and center parts demonstrate how identical states can be generated from different original hole positions. Arrows represent the hopping of the hole; crosses enclosed in ellipses denote quantum fluctuations. The hopping part of the Hamiltonian is represented by a curved arrow, the exchange part by two crosses. In Fig. 1 explicit spin configurations related to Figs. 2(a)–2(e) have

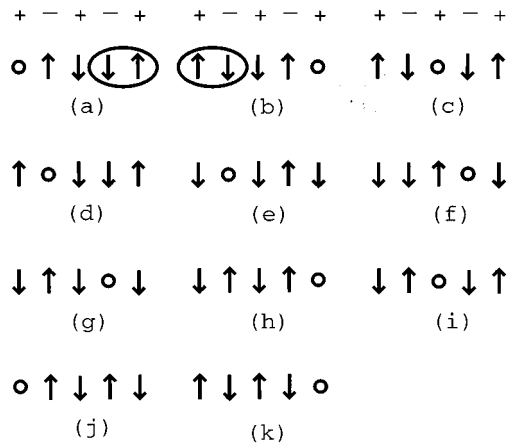

FIG. 1. Spin configurations related to some contributions to overlap and Hamilton matrices.

been shown. The sequence of plus and minus signs represents directions of the staggered magnetic field. Ellipses again denote quantum spin fluctuations which are present in the ground state of the model at half-filling.

In Fig. 2(a) a process which contributes to $N_{i,j}^{\tau_i,\tau_j}$ has been depicted. It involves a quantum fluctuation of the ''spin background'' $|AF\rangle$. Figures 1(a) and 1(b) represent original configurations which correspond to the left and central parts of Fig. 2(a). In Fig. 1(c) the final common spin configuration which was formed after two hops of each hole has been plotted. The process described by the diagram in Fig. 2(a) contributes to the matrix element $\langle \Psi_i^m | \Psi_{i+4}^n \rangle$. It follows from Eqs. (3), (A4), and (A6) that the corresponding contribution is $\lambda_0^2 \alpha_2^m \alpha_2^n$. The factor λ_0^2 is related to the presence of quantum fluctuations in the left and middle parts of Fig. 2(a) while the factor $\alpha_2^m \alpha_2^n$ to the fact that the states which correspond to them have been obtained by two jumps of each hole. For further examples of the numerical computation of matrix elements we refer the reader to Refs. 8, 9, and 12. For the sake of brevity we shall skip their further analysis in the present paper. Figure 2(b) represents the corresponding contribution to the Hamiltonian matrix $H_{i,j}^{\tau_i,\tau_j}$. The application of the kinetic part of the Hamiltonian to the state depicted in the middle part of Fig. 2(a), which corresponds to the factor α_2^i in Eq. (3) and the configuration plotted in Fig. 1(c), leads to the state depicted in the left part of Fig. 2(a), which corresponds to the factor α_1^i in Eq. (3) and the configuration plotted in Fig. 1(d). In Fig. 2(c) the dominant process for hole propagation due to the *transverse part* of the Heisenberg Hamiltonian (H_1) has been represented. In the left part of it the state obtained from the spin configuration plotted in Fig. 1(e) by two jumps of a hole has ben depicted. It corresponds to the factor α_2^i in Eq. (3) and the configuration plotted in Fig. 1(f). The action of the Heisenberg Hamiltonian on the state which corresponds to the spin configuration depicted in Fig. 1(g) leads to the state represented by the central part of Fig. 2(c), equivalent to the left part of it and the configuration in Fig. 1(f). Figures 2(d) and Fig. 2(e) represent similar processes which, however, involve quantum fluctuations in the ground state of the Hamiltonian (1) at half-filling and thus may be of minor importance. The starting configuration which corresponds to the central part of Fig. 2(d) has been depicted in Fig. 1(h). The configuration plotted in Fig. 1(i) corresponds to both wave functions represented by the left and middle parts of Fig. 2(d). The starting configuration for the left part of Fig. 2(e) has been plotted in Fig. 1(j), while the common final configuration for the left and central parts of it in Fig. 1(k).

We restrict our considerations to processes which maximally involve four spin defects. Terms in the expansion which correspond to higher number of defects are likely to have smaller contribution.

The coefficients $\beta_{i,j}^{\rho}$ for a two-hole wave function with momentum k take the form $e^{ikR_i}\beta_{j-i}^{\rho}$. For simplicity we assume that the factorization (5) for the $\alpha_{\mu,\nu}$ is valid unless i and j are nearest neighbors. In the latter case we have to solve a new kind of Schrödinger equation, as shown in the Appendix.

Figure 3 then represents various processes which lead to nontrivial contributions to the overlap $N_{i,j}^{\tau_i,\tau_j}$ matrix for two holes. Figures 3(a)–3(d) show how the same state can be created by hopping of two holes originally created at two different nearest-neighbors sites. Figures 3(e) and 3(f) represent processes which involve a quantum fluctuation.

In Fig. 4 contributions related to the kinetic part of the Hamiltonian have been depicted. Diagrams in Figs. 4(a)-4(c) represent corrections which have to be made because one hole ''blocks'' the hopping of the second hole. Hopping processes indicated in the central column are impossible if the respective ''final site'' is occupied by the second hole, so that the corresponding gain in kinetic energy has to be sub-

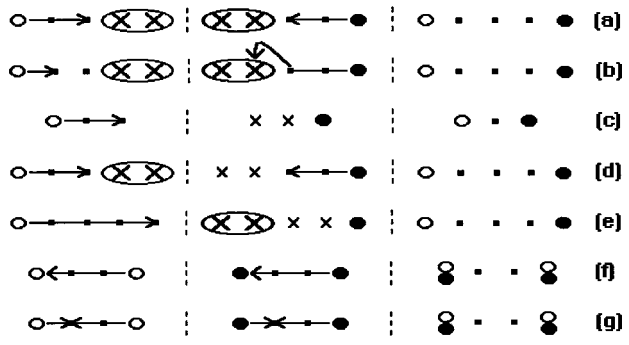

FIG. 2. Processes which contribute to the overlap and Hamiltonian matrices in the case of a single hole.

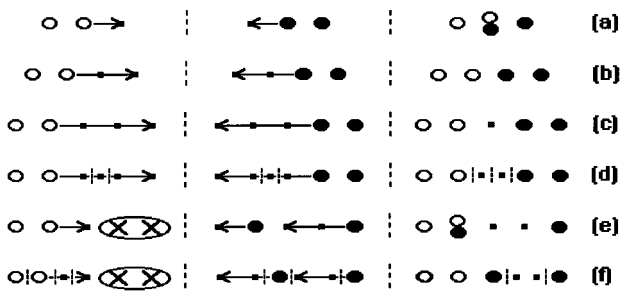

FIG. 3. Processes which contribute to the overlap matrix in the case of two holes.

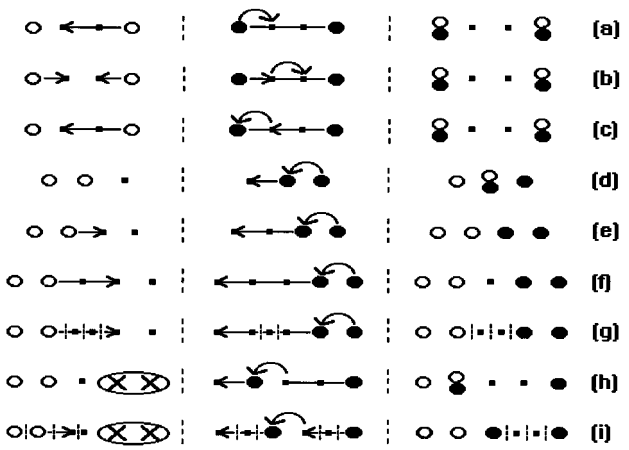

FIG. 4. Processes related to the kinetic part of the Hamiltonian in the case of two holes.

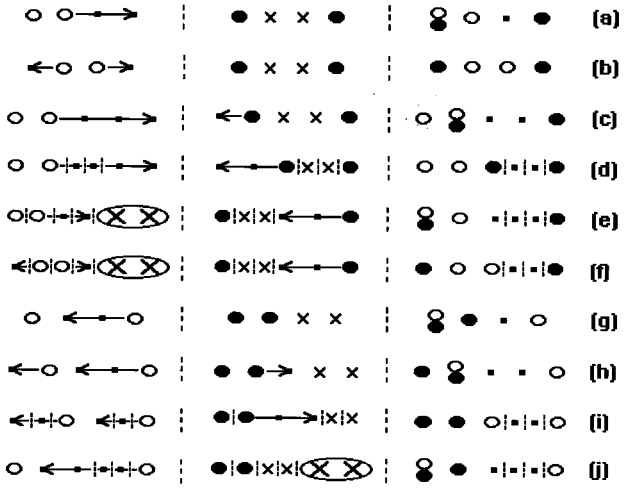

FIG. 6. Processes related to H_1 in the case of two holes.

tracted from the estimate (6). Figures 4(d)–4(i) represent some processes which yield nontrivial off-diagonal matrix elements of the the kinetic part of the Hamiltonian H_t. Figure 5 represents some necessary subtractions connected to the part H_{Ising} of the Hamiltonian (1): When two holes occupy nearest-neighbor sites there is a change of the exchange energy which needs to be accounted for. Finally, Fig. 6 shows processes which involve the transverse part of the Heisenberg Hamiltonian H_1.

We proceed to the case of three holes. Our considerations are restricted to states with $S_z=1/2$, i.e., with one hole created in the spin up sublattice and two in the spin down sublattice. The general form of the solution of Eq. (8) with momentum k is $\beta_{j-i,n-i}e^{ikR_i}$. To keep the calculation manageable we also restricted the possible configurations to states with maximally two ''spin defects'' (i.e., spins overturned with respect to the Néel state) and took into account only ground states of Eq. (4). In the case of diagonal contributions related to corrections to the ''Ising part'' of the eigenenergies E_τ which are caused by presence of another hole only ''paths'' with one spin inverted have been taken into account. We also neglected corrections to the overlap originating from paths which consist of more than one overturned spin. In Figs. 7(a)–7(n) processes which involve three holes have been depicted. Figures 7(a)–7(b) represent contributions to the overlap matrix which are a three hole version of processes shown in Figs. 3(a)–3(c). Figures 7(d)–7(f) represent corrections to the ''Ising part'' of energy which are caused by the presence of an additional hole. In Figs. 7(g) and 7(j) processes which are related to the kinetic part of the Hamiltonian have been presented. They are similar to their counterparts which involve only two holes and were depicted in Figs. 4(d) and 4(e). Processes which are related to the transverse part of the Heisenberg Hamiltonian and involve three holes have been represented by diagrams (k)–(n) in Fig. 7.

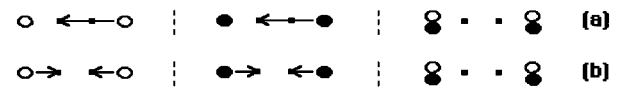

FIG. 5. Diagrams which correspond to corrections related to the Ising part of the Hamiltonian in the case of two holes.

III. COMPARISON BETWEEN NUMERICAL AND ANALYTICAL RESULTS

In the following we compare results for a 16-site ring with periodic boundary conditions, obtained by the variational calculation and by exact diagonalization. We set $h=J/2$ and $t=1$. We begin with the energy dispersion of a single hole, shown in Fig. 8. Thereby the energy of the half-filled ground state has been subtracted and the variational band rigidly shifted downwards by a value of order J (approximately $0.05t=0.25J$ for $J/t=0.2$). The negative sign of the shift indicates that the rise in energy due to the destruction of the spin arrangement is slightly overestimated in our approach. The failure of the variational approach to reproduce accurately the *absolute* position of the band is most probably due to inaccuracies in the values of ''spin bag'' eigenenergies

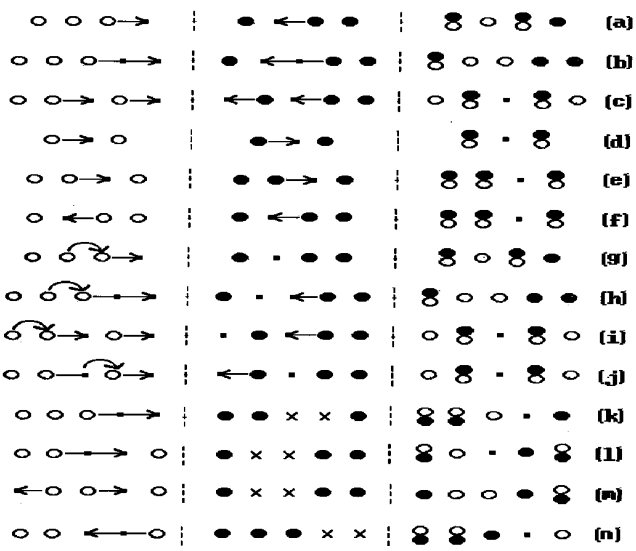

FIG. 7. Processes intrinsic for the three hole case.

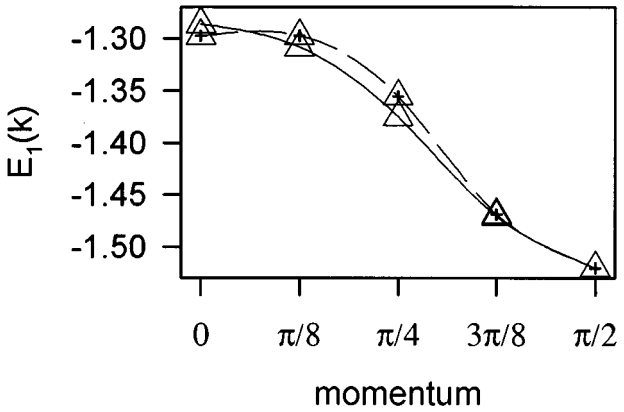

FIG. 8. Energy dispersion for the 16-site ring by exact diagonalization (triangles) and variational calculation (crosshaired triangles), $J/t=0.2$.

which were obtained by solving the Schrödinger equation (4). On the other hand, the variational method describes the energy dispersion very well: The agreement for the lowest-band dispersion is very good in the whole range of parameters under consideration ($0.1t \leqslant J \leqslant 1.2t$, $h=J/2$). The main contribution to the lowest-band wave functions comes from the ground state of the self-trapped hole problem (4); while higher-lying eigenstates of Eq. (4) have little weight in the wave functions (7) of this band, they are relevant to the dispersion of the expectation value of the kinetic energy, shown in Fig. 9. The broad analytical band which agrees very well with the numerical result has been calculated in the basis of the five lowest functions $\tilde{\alpha}_\nu^\tau$ while for the narrow band only the $\tau=0$ wave function has been retained.

We proceed to the case of two holes. The form of the lowest bands [see Figs. 10(a) and 10(b)] is again well predicted by the variational calculation. Each variational band has been adjusted to its numerical counterpart at one single point; the downward shifts of the individual bands by a fraction of J were nearly the same. The dispersion of the kinetic energy [Fig. 10(c)] also agrees well with the variational calculation.

We next consider the density-density correlation function

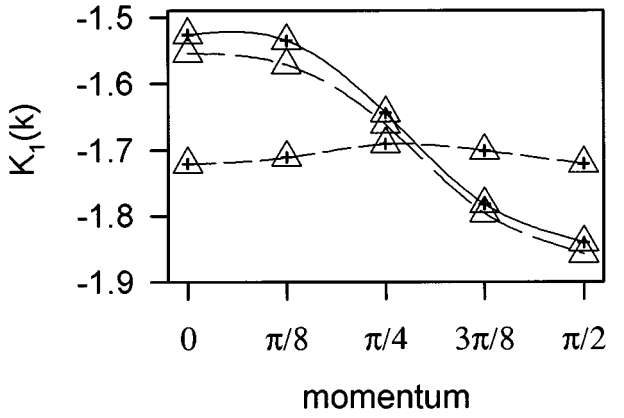

FIG. 9. Ground state kinetic energy dispersion for a single hole ($J=0.7t$, $h=J/2$) by exact diagonalization (triangles) and variational approach (crosshaired triangles).

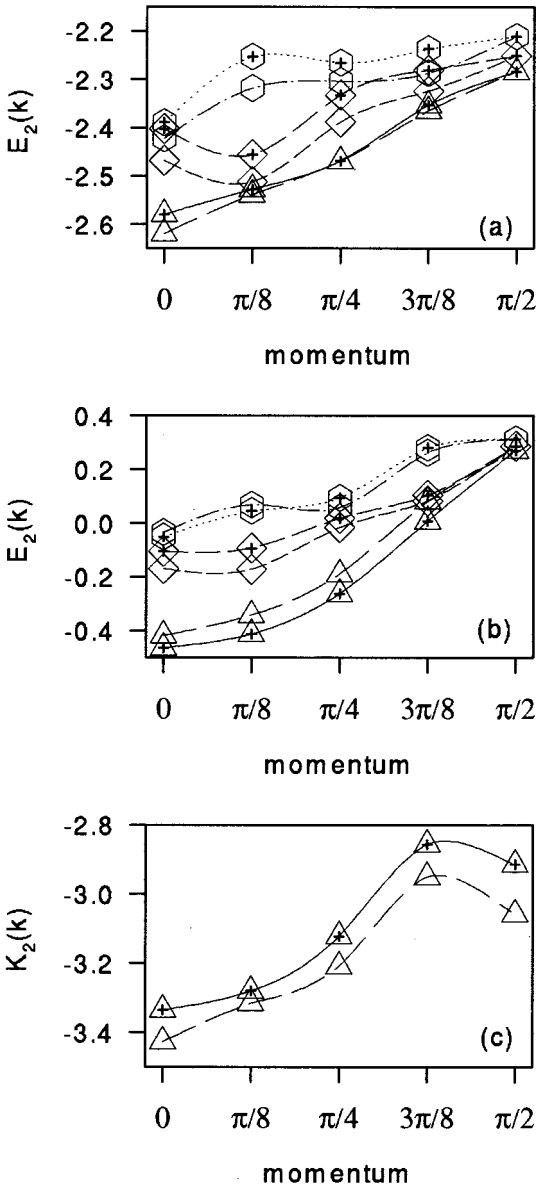

FIG. 10. (a) Dispersion of the three lowest bands for two holes by exact diagonalization (polygons) and variational approach (crosshaired polygons), $J/t=0.3$. (b) Dispersion of the three lowest bands for two holes by exact diagonalization (polygons) and variational approach (crosshaired polygons), $J/t=0.9$. (c) Dispersion of the kinetic energy for two holes, $J/t=1$.

$$g(r_d)=\sum_s \langle n_{hs} n_{hs+r_d} \rangle. \tag{11}$$

The index s runs over all sites for $r_d \neq N/2$ and over a half of them for $r=N/2$. The function $g(r)$ provides a criterion for hole binding. Figure 11(a) shows $g(r_d)$ for two opposite situations. The shape of the curves which reach their maximum in the left part of the figure drawn for $J/t=0.7$ obviously indicates the formation of a bound state, whereas those curves which have maxima at the right part of the figure ($J/t=0.1$) suggest repulsion between the holes in the corresponding parameter region. The agreement between the numerical and analytical approaches is very good for small values of J; for higher values of J the variational result correctly indicates the tendency towards binding and the po-

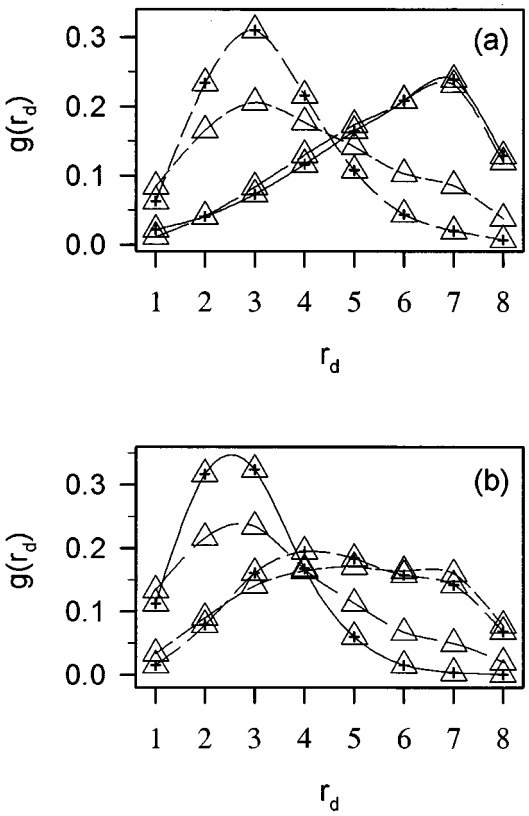

FIG. 11. (a) Hole density-density correlation function for $J/t=0.7$ (curves which culminate at the distance 3) and for $J/t=0.1$ (curves which culminate at the distance 7). (b) Hole density-density correlation function for $J/t=0.9$ (curves peaked at distances 2 and 3) and for $J/t=0.4$.

sition of the maximum in $g(r_d)$. The variational results, moreover, predict correctly the parameter range where two holes start to form a bound state as demonstrated in Fig. 11(b) for the intermediate case of $J/t=0.4$. In addition to the density-correlation function the variational calculation offers a more direct check for hole binding, namely, the form of the wave function β^{ρ}_{j-i}. We recall that the indices i and j may be thought of as the ''centers of gravity'' of the spin bag quasiparticles. Then, the probability distribution $|\beta^{\rho}_n|^2$ is shown in Fig. 12 for $J/t=0.4$ and momentum $p=0$. We

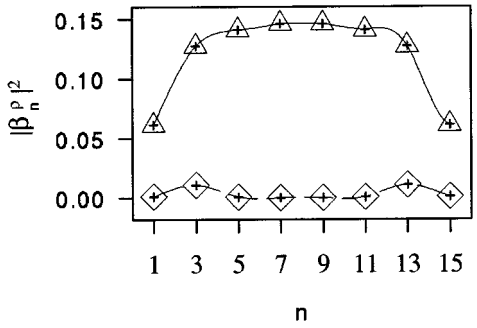

FIG. 12. Amplitudes $|\beta^{\rho}_n|^2$ as a function of distance n for $J/t=0.4$ and momentum $p=0$. Crosshaired triangles correspond to $\rho=1$ for $n=1,15$ or $\rho=(1,1)$ for $n=3,5,\ldots,13$. Crosshaired diamonds represent values of $|\beta^{\rho}_n|^2$ for $\rho=2$ and $n=1,15$ or $\rho=(1,2),(2,1)$ and $n=3,5,\ldots,13$.

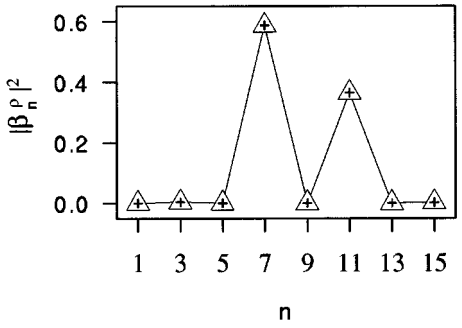

FIG. 13. Amplitudes $|\beta^{\rho}_n|^2$ as a function of distance n for $J/t=0.5$, momentum $p=\Pi/2$ and $\rho=1$, $n=1,15$ or $\rho=(1,1)$, $n=3,5,\ldots,13$.

have used a basis which consists of two lowest states for both single- and two-hole string bags. For spin bags on nearest neighbors, i.e., $n=1,15$, the index ρ can have two possible values 1 and 2 while for more distant spin bags, i.e., $n=3,5,\ldots,13$, ρ is actually a pair of indices, $\rho=(i,j)$, where $i,j=1,2$. Crosshaired triangles correspond to $\rho=1$ for $n=1,15$ or $\rho=(1,1)$ for $n=3,5,\ldots,13$. Crosshaired diamonds represent the values of $|\beta^{\rho}_n|^2$ for $\rho=2$ and $n=1,15$ or $\rho=(1,2),(2,1)$ and $n=3,5,\ldots,13$. The contribution from states which correspond to $\rho=(2,2)$ and $n=3,5,\ldots,13$ is negligible in the case of the ground state and has been omitted in Fig. 12. There is a rather clear correspondence between the hole density-density correlation function in Fig. 11(b) and the plot of $|\beta^{\rho}_n|^2$. The ''self trapped'' hole wave functions obviously form a natural basis for the description of coherent motion and interaction of quasiparticles. We see from Fig. 12 that in the ground state at $J/t=0.4$ all possible distances between the self-trapped hole have comparable probability. On the other hand, $|\beta^{\rho}_n|^2$ has a substantial value only for $\rho=1,(1,1)$ which indicates only weak mixing of different ''orbitals.'' By plotting $|\beta^{\rho}_n|^2$ for different values of J we can trace the transition between the independent hole and bound state regimes. For large J the amplitudes $|\beta^{\rho}_n|^2$ have their maximum value at $n=1,15$ whereas for small J the maximum is at $n=7,9$. It is interesting to note that for intermediate values of J and momentum $p=\pi/2$ the quasiparticle wave function has a special form, shown in Fig. 13 for $J/t=0.5$. In this figure $\rho=1$ for $n=1,15$ or $\rho=(1,1)$ for $n=3,5,\ldots,13$ ($|\beta^{\rho}_n|^2$ for other values of ρ is negligible). We see that the wave function corresponds to two spin bags centers of which lie at sites separated by 7 and 5 (11) lattice spacings. We have also calculated the hole density-density correlation function for $p=\pi/2$ and $J/t=0.5$ in order to check whether the nontrivial form of Fig. 13 is correct. The result is shown in Fig. 14. Triangles and crosshaired triangles up correspond as usually to numerical diagonalizations and variational calculations, respectively. The good agreement demonstrates that the single-hole ''orbitals'' as predicted by the string approach are true objects whose existence is indirectly manifested by the properties of weakly doped antiferromagnets. As a further check we have done an additional calculation in which matrix elements which correspond to the processes which couple two above mentioned relevant wave functions have been omitted. This leads to a solution

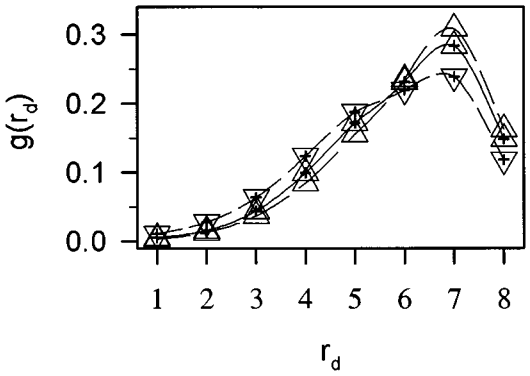

FIG. 14. Hole density-density correlation function for $J/t=0.5$ and momentum $p=\Pi/2$. Crosshaired triangles down correspond to a calculation with some processes neglected.

where $|\beta_n^\rho|^2$ is almost equal at $n=7$ and $n=11$ while for other values of n it is again negligible. The resulting density correlation function is given by crosshaired triangles down in Fig. 14 and is slightly different from the density correlation function obtained by means of the numerical calculation. It shows that the solution represented by Fig. 13 is very accurate and even processes which involve several spin ''defects'' like those omitted in the additional check calculation may be of real importance.

Despite the inaccuracy of the absolute energy values we proceed to a discussion of the binding energy of two holes. It is defined as

$$\epsilon_b=\epsilon_{2h}-2\epsilon_{1h}+\epsilon_{0h}, \tag{12}$$

where ϵ_{ih} denotes the ground state energy with i holes. That quantity is shown in Fig. 15. Due to errors in the estimation of the spin bag ''orbital'' energy, the critical J where binding occurs would be predicted too large by considering only the binding energy. The ''quasiparticle wave function'' $\beta_{i,j}^\rho$ therefore is a much better indicator for the tendency towards binding because the shift of its maximum from longer distance to shorter distance occurs at the correct value of J/t for hole binding.

We next consider the case of three holes. Figure 16 shows

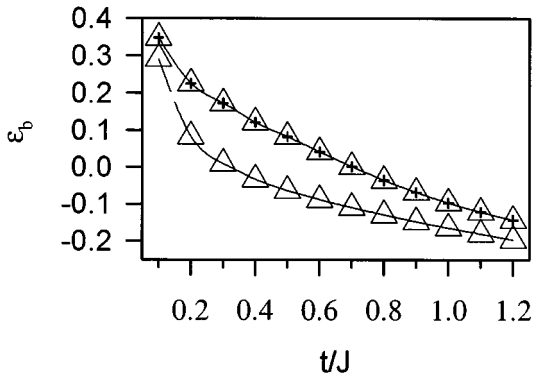

FIG. 15. Binding energy ϵ_b in units of J as a function of ratio J/t obtained by means of exact diagonalization (smaller triangles) and the variational approach (larger triangles).

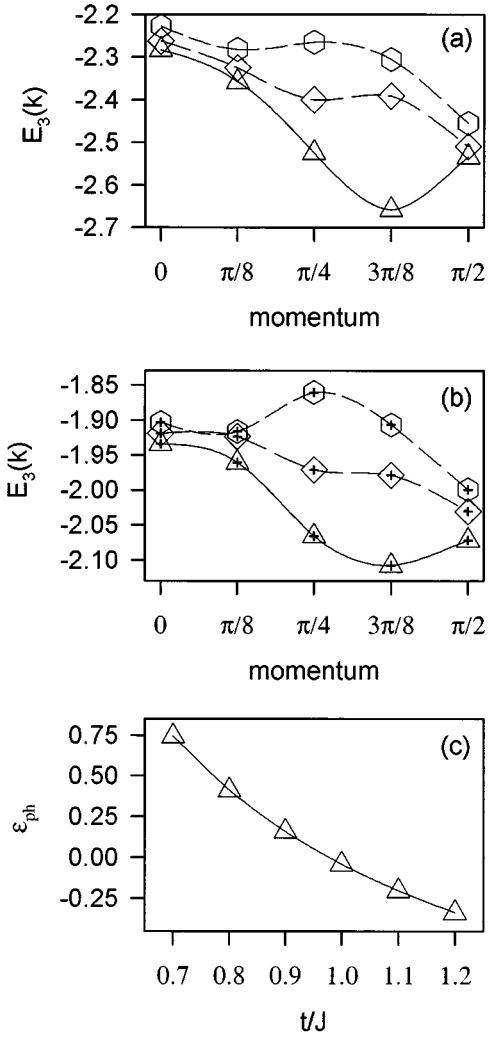

FIG. 16. Energy dispersion for the three lowest bands for three holes by (a) exact diagonalization and (b) variational calculation. $J/t=0.5$. (c) ''Phase separation energy'' vs J/t.

the three lowest energy bands. Despite some differences which concern bandwidths and curve shapes, the band structure derived by the variational approach is quite similar to that obtained in the exact diagonalization. This indicates that even multihole states of antiferromagnets doped with about 20% of holes may be reasonably well described by the string picture. In the calculation for three holes we have taken into account only processes which involve two spin defects in the Néel background. From previous considerations we know that for better accuracy one would have to take into account states which incorporate much larger number of inverted spins. On the other hand, the main source of errors in our method is the inaccuracy of the spin bag wave function eigenenergy, which in the single- and two-hole cases influence the band positions.

By analyzing the results for three-hole states we can draw conclusions about the possibility of phase separation. The stability of a three-hole bound state against the decay into a hole pair and an isolated hole is a necessary (but not sufficient) condition for phase separation. We therefore define the ''phase separation energy'' $\epsilon_{\rm ph}$:

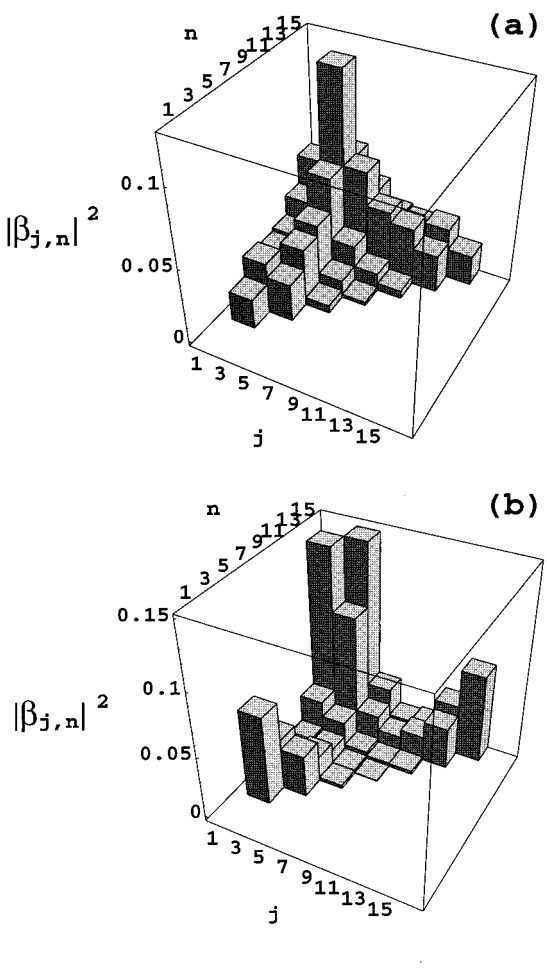

FIG. 17. (a) Amplitudes $|\beta_{j,n}|^2$ as a function of distances j and n for $J/t=0.9$. (b) Amplitudes $|\beta_{j,n}|^2$ as a function of distances j and n for $J/t=1.1$.

$$\epsilon_{\mathrm{ph}}=\epsilon_{3h}-\epsilon_{2h}-\epsilon_{1h}+\epsilon_{0h}\,. \tag{13}$$

Numerical values for ϵ_{ph} are given in Fig. 16(c). The three-hole bound state becomes stable for $J\approx 1$. As mentioned before the variational approach is prone to errors in the absolute values of energies. As a more reliable criterion for phase separation we thus again use the wave function $\beta_{j,n}$. As discussed previously the self-trapped holes are the natural starting point for the description of the doped antiferromagnet. They are the ''effective particles'' seen in numerical experiments. Therefore it is natural to discuss hole binding or phase separation not in terms of ''bare'' holes, but in terms of these effective particles, and $|\beta_{j,n}|^2$ is directly connected to the density correlation function for those particles. Then, Fig. 17 shows $|\beta_{j,n}|^2$ as a function of distances j and n for $J/t=0.9$ and $J/t=1.1$, respectively. The values of J have been chosen on both sides of the transition determined by the value of J where ϵ_{ph} changes sign. In Fig. 17(a) we see that in the ground state for $J/t=0.9$ ($p=3/8\Pi$) configurations with a pair of self-trapped holes separated by one or three lattice spacings and the third hole which occupies an arbitrarily distant site have the largest weights. This situation changes completely for $J/t=1.1$. In Fig. 17(b) we see that larger bars concentrate around corners of the triangle. This is a clear manifestation of a tendency towards minimization of the distances between effective particles which is an indication of phase separation.

IV. CONCLUSIONS

In summary, we have demonstrated that the variational approach based on the string picture is an appropriate language for discussion of weakly doped antiferromagnet properties. In some cases the ground state has an extraordinarily simple and transparent form in the language of spin bag wave functions, its correctness being demonstrated by rather detailed agreement with numerical results. Tendencies towards binding or phase separation in different parameter regions are clearly manifested in the language of dressed holes. Both numerical and analytical calculations indicate that binding is dominating in a broad domain of parameters; however, for large values of the superexchange parameter J the formation of larger hole clusters and (probably) phase separation[15] takes place. The effective Hamiltonian constructed by means of the string picture appears to be a correct description of low-energy physics in weakly doped antiferromagnets. Provided that the t-J model itself has some relevance to the copper oxides it may serve as a candidate for the description of their properties at least in the underdoped regime.

Experimental evidence for the proposal that the magnetic interaction between planar quasiparticles in the cuprate superconductors is responsible for both their anomalous normal state behavior and their transition at high temperature to a superconducting state with $d_{x^2-y^2}$ pairing is growing. A phenomenological ''Urbana model''[16,17] seems to be a promising step towards understanding of high T_c compound properties in terms of a nearly antiferromagnetic Fermi liquid. The effective Hamiltonian considered in that paper might serve as a basis for attempts to find connections between that phenomenological model and widely discussed in the context of HTSC oneband and multiband Hubbard-like models.

ACKNOWLEDGMENTS

P.W. acknowledges partial financial support from the Scientific Research Council (KBN). Support of R.E. by the European Community is gratefully acknowledged.

APPENDIX

In the lowest approximation we will write the Schrödinger equation for Eq. (1) in the subspace which corresponds to holes localized at a site i and is spanned by functions of the form (3). We start from a prescription for the calculation of some matrix elements

$$\langle AF|A^{\dagger}_{i,\nu}A_{j,\mu}|AF\rangle, \tag{A1}$$

$$\langle AF|A^{\dagger}_{i,\nu}\mathcal{L}A_{j,\mu}|AF\rangle, \tag{A2}$$

where $\mathcal{L}$ is the Liouville operator given by

$$\mathcal{L}B=[H,B]_-\,. \tag{A3}$$

In a paper by Becker and Brenig[18] a cumulant-based tool for such calculations has been invented. It is founded on the formulas

$$\langle \hat{O} \rangle = \langle \Omega^{\dagger} \hat{O} \Omega \rangle_0^c, \tag{A4}$$

$$\Omega = 1 + \lim_{x \to 0} \frac{1}{x - (\mathcal{L}_0 + H_1)} H_1. \tag{A5}$$

$\langle \hat{O} \rangle$ denotes the expectation value calculated for the ground state of the total Hamiltonian $H = H_0 + H_1$. $\langle \cdots \rangle_0^c$ is a cumulant matrix element calculated for the ground state of the unperturbed Hamiltonian H_0. In our case $H_0 = H_t + H_{\mathrm{Ising}}$. By neglecting in Ω higher powers of a pair contribution $(J/2) S_i^- S_j^+$ which correspond to the same pair of states one gets an approximated form of it:

$$\Omega \approx \prod_{\langle i,j \rangle} (1 + \lambda_0 S_i^- S_j^+); \quad \lambda_0 = -\frac{1}{2 + 4h/J}. \tag{A6}$$

The subscripts ''i,m'' and ''j,n'' correspond here and in the following considerations to the ''spin up'' and ''spin down'' sublattices, respectively. That type of approximation motivated by the form of the so-called Bartkowski wave function[19] has been suggested in a paper by Becker *et al.*,[20] for the 2D t-J model. The variational approach used in our considerations is equivalent to a simplest version of the projection technique in the formulation introduced by Becker and Fulde[21,22] and may be refined by application of the full projection formalism.

All expectation values in subsequent calculations will be factorized according to

$$\left\langle \prod_{\langle mn \rangle} [1 + \lambda_0 (S_m^+ S_n^-)] B \prod_{\langle ij \rangle} [1 + \lambda_0 (S_i^- S_j^+)] \right\rangle_0^c \cong \prod_{\langle ij \rangle \in \mathcal{B}} \langle [1 + \lambda_0 (S_i^+ S_j^-)] B [1 + \lambda_0 (S_i^- S_j^+)] \rangle_0^c, \tag{A7}$$

where B is a dimensionless particle-number-conserving combination of creation and annihilation operators. $\mathcal{B}$ is the set of bonds connected to sites related to B. The relation (A7) is rigorous up to second order in λ_0 and should not lead to any important errors. In that approximation one gets from Eq. (A2) a set of useful relations. They implicitly lead to a Schrödinger equation which describes a hole trapped at site i:

$$-t[(1-\lambda_0^2)^{(1-\delta_{\nu,0}-\delta\nu,-1)\mathrm{sgn}(|\nu+1|-|\nu|)} \tilde{\alpha}_{\nu+1} + (1-\lambda_0^2)^{(1-\delta_{\nu,0}-\delta\nu,1)\mathrm{sgn}(|\nu-1|-|\nu|)} \tilde{\alpha}_{\nu-1}]$$
$$+ \left[(\tfrac{3}{2} - \tfrac{1}{2}\delta_{\nu,0}) J + (\tfrac{1}{2} + |\nu|) h - \frac{J}{2} \frac{\lambda_0}{1-\lambda_0^2} (3 + |\nu| + \delta_{\nu,0}) \right] \tilde{\alpha}_{\nu} = E_1 \tilde{\alpha}_{\nu}. \tag{A8}$$

In a similar way one can write a Schrödinger equation for two holes trapped at two nearest-neighbor sites. In the lowest approximation we assume that each hole is forbidden to retrace the path of the second hole. Therefore the coefficient $\alpha_{-\mu,\nu}^{i,i+1} \equiv \tilde{\alpha}_{\mu,\nu}$ does not vanish only for non-negative μ and ν. We then obtain a Schrödinger equation for two holes trapped at two nearest-neighbor sites:

$$-t[(1-\lambda_0^2)^{(1-\delta_{\mu,0})} \tilde{\alpha}_{\mu+1,\nu} + (1-\lambda_0^2)^{-(1-\delta_{\mu,1})} \tilde{\alpha}_{\mu-1,\nu} + (1-\lambda_0^2)^{(1-\delta_{\nu,0})} \tilde{\alpha}_{\mu,\nu+1} + (1-\lambda_0^2)^{-(1-\delta\nu,1)} \tilde{\alpha}_{\mu,\nu-1}]$$
$$+ \left[(2 - \tfrac{1}{2}\delta_{\mu+\nu,0}) J + (1 + \mu + \nu) h - \frac{J}{2} \frac{\lambda_0}{1-\lambda_0^2} [3 + \mu + \nu + (\delta_{\mu,0} + \delta_{\nu,0})] \right] \tilde{\alpha}_{\mu,\nu} = E_2 \tilde{\alpha}_{\mu,\nu}. \tag{A9}$$

For three holes trapped at nearest-neighbor sites we may proceed in a similar way. Again we consider in the lowest order a Schrödinger equation in a restricted Hilbert space defined by a condition that no hole is allowed to retrace the path of another hole, which is equivalent to a condition that $\alpha_{-\mu,\nu,\eta}^{i,j,n} \equiv \tilde{\alpha}_{\mu,\nu,\eta}^{i,i+1,i+2}$ does not vanish only if $\mu \geqslant 0, \nu = 0, \eta \geqslant 0$. In all other cases, when three holes are not trapped at nearest-neighbor sites, the coefficients $\alpha_{\mu,\nu,\eta}^{i,j,n}$ are products of $\tilde{\alpha}_{\ldots}$ or $\tilde{\alpha}_{\ldots,\ldots}$. The Schrödinger equation for $\tilde{\alpha}_{\mu,\nu,\eta}^{i,i+1,i+2}$ is given by

$$-t[(1-\lambda_0^2)^{(1-\delta_{\mu,0})} \tilde{\alpha}_{\mu+1,0,\nu} + (1-\lambda_0^2)^{-(1-\delta_{\mu,1})} \tilde{\alpha}_{\mu-1,0,\nu} + (1-\lambda_0^2)^{(1-\delta_{\nu,0})} \tilde{\alpha}_{\mu,0,\nu+1} + (1-\lambda_0^2)^{-(1-\delta_{\nu,1})} \tilde{\alpha}_{\mu,0,\nu-1}]$$
$$+ \left[\left(3 - \frac{1}{2}(\delta_{\mu,0} + \delta_{\nu,0}) \right) J + (\tfrac{3}{2} + \mu + \nu) h - \frac{J}{2} \frac{\lambda_0}{1-\lambda_0^2} [4 + \mu + \nu + (\delta_{\mu,0} + \delta_{\nu,0})] \right] \tilde{\alpha}_{\mu,0,\nu} = E_3 \tilde{\alpha}_{\mu,0,\nu}. \tag{A10}$$

*Also at Institute of Low Temperature and Structure Research, P.O. Box 937, 50-950 Wrocław 2, Poland.

[1] P. Prelovšek, I. Sega, and J. Bonča, Phys. Rev. B **39**, 7074 (1989).
[2] Y. Hasegawa and D. Poilblanc, Phys. Rev. B **40**, 9035 (1989).
[3] E. Dagotto, J. Riera, and A. P. Young, Phys. Rev. B **42**, 2347 (1990).
[4] P. A. Bares and G. Blatter, Phys. Rev. Lett. **64**, 2567 (1990); B. Sutherland, Phys. Rev. B **12**, 3795 (1975).
[5] H. J. Schulz, Phys. Rev. Lett. **64**, 2831 (1990).
[6] M. Ogata, M. Luchini, S. Sorella, and F. F. Assaad, Phys. Rev. Lett **66**, 2388 (1991).
[7] J. Bonča, P. Prelovšek, I. Sega, H. Q. Lin, and D. K. Campbell, Phys. Rev. Lett. **69**, 526 (1992).
[8] R. Eder, Phys. Rev. B **45**, 319 (1992).

[9] P. Wróbel and R. Eder, Phys. Rev. B **49**, 1233 (1994).
[10] M. Bonisegni and E. Manousakis, Phys. Rev. B **43**, 10 353 (1991); D. Poilblanc, J. Riera, and E. Dagotto, *ibid.* **49**, 12 318 (1994).
[11] A. Moreo and Daniel Duffy, Phys. Rev. B **51**, 11 882 (1995).
[12] R. Eder and P. Wróbel, Phys. Rev. B **47**, 6010 (1993).
[13] L. N. Bulaevskii, E. L. Nagaev, and D. L. Khomskii, Sov. Phys. JETP **27**, 836 (1968).
[14] B. I. Shraiman and E. D. Siggia, Phys. Rev. Lett. **60**, 740 (1988).
[15] S. V. Kivelson, V. Emery, and H. Q. Lin, Phys. Rev. B **42**, 6523 (1990).
[16] P. Monthoux, A. Balatsky, and D. Pines, Phys. Rev. B **46**, 14 803 (1992).
[17] P. Monthoux and D. Pines, Phys. Rev. B **47**, 6069 (1993).
[18] K. W. Becker and W. Brenig, Z. Phys. B **79**, 195 (1990).
[19] R. R. Bartkowski, Phys. Rev. B **5**, 4436 (1972).
[20] K. W. Becker, R. Eder, and H. Won, Phys. Rev. B **45**, 4864 (1992).
[21] K. W. Becker and P. Fulde, J. Chem. Phys. **91**, 4223 (1989).
[22] P. Fulde, *Electron Correlations in Molecules and Solids*, Springer Series in Solid-State Science, Vol. 100 (Springer, Berlin, 1991).